PAPER

Metal loading determines the stabilization pathway for Co²⁺ in titanate nanowires: ion exchange *vs.* cluster formation

D. Madarász,[a] G. Pótári,[b] A. Sápi,[a] B. László,[b] C. Csudai,[b] A. Oszkó,[b] Á. Kukovecz,[ac] A. Erdőhelyi,[b] Z. Kónya[ad] and J. Kiss*[bd]

Co nanoparticles were produced and characterized on protonated titanate nanowires. Co deposits were obtained after low-temperature decomposition of $Co_2(CO)_8$ on titanate nanostructures. The carbonylation was carried out by vapor-phase adsorption in a fluidized bed reactor and the decarbonylation processes were followed by FT-IR spectroscopy and microbalance combined with temperature programmed reaction mass spectrometry. The band gap of Co-decorated titanate nanostructures determined by UV-VIS diffuse reflectance spectroscopy decreased sharply from 3.14 eV to 2.41 eV with increasing Co content up to 2 wt%. The Co-decorated titanate morphology was characterized by high-resolution transmission electron microscopy (HRTEM) and electron diffraction (ED). The chemical environment of Co deposition was studied by photoelectron spectroscopy (XPS). A certain amount of cobalt underwent an ion exchange process. Higher cobalt loadings led to the formation of nanosized-dispersed particles complexed to oxygen vacancies. The average sizes were found to be mostly between 2 and 6 nm. This size distribution and the measured band gap could be favorable regimes for some important low-temperature thermal- and photo-induced catalytic reactions.

Introduction

High aspect-ratio TiO_2 and titanate nanostructures are being intensively studied at present because of their promising photoelectrical,[1,2] biomedical,[3] and Li⁺ and hydrogen storage properties.[4–6] Organic photovoltaics (OPVs) incorporated with TiO_2 nanowires show lower energy disorder, improved charge transport, more balanced electron–hole mobility and enhanced performance.[7] In addition, nanostructured titanates have impressive mechanical properties.[8] Recently, a comprehensive review[9] and a study[10] about the fabrication, modification and application of titania nanoobjects were published.

Titanate nanotubes are open-ended hollow tubular objects measuring 7–10 nm in outer diameter and 50–170 nm in length. They feature a characteristic spiral cross-section composed of 4–6 wall layers. The typical diameter of their inner channel is 5 nm.[11,12] Titanate nanowires represent the thermodynamically most stable form of sodium trititanate under the alkaline hydrothermal conditions applied in titanate nanotube synthesis as well. (Note that the post-synthetic neutralization step converts the original $Na_2Ti_3O_7$ into its hydrogen form without affecting the nanowire morphology.) Their diameter is 45–110 nm and their length is between 1.8 and 5 μm.[13] The specific surface area of titanate nanotubes is rather large ($\sim$185 m^2 g^{-1}) due to their readily accessible inner channel surface, whereas that of titanate nanowires is $\sim$20 m^2 g^{-1}. According to our independent infrared spectroscopic (IR), thermogravimetric and X-ray diffraction (XRD) measurements as well as findings[14] in the literature, the trititanate structure appears to be thermally deconstructed at approx. 573 K. Annealing at higher temperatures initiates the trititanate to the anatase conversion process.

Titanate nanoobjects are of great interest for catalytic applications, since their high cation exchange capacity enables high metal (*e.g.* Co, Cu, Ni, Ag) loadings and dispersion.[15,16] Ion exchange also allows titanate nanostructures to incorporate metal adatoms into their framework which may create another type of active center besides metal clusters. Studies in this direction are still scarce in the literature because of the genuine novelty of the titanate nanomaterial based non-photocatalytic heterogeneous catalysis field.

Very recently it was found that nanowires and nanotubes could stabilize gold and rhodium in a dispersed form (1.5–5 nm).[17–21]

[a] *Department of Applied and Environmental Chemistry, University of Szeged, Hungary*

[b] *Department of Physical Chemistry and Materials Science, University of Szeged, Aradi vértanúk tere 1., H-6720 Szeged, Hungary. E-mail: jkiss@chem.u-szeged.hu; Fax: +36 62 546482; Tel: +36 62 544803*

[c] *MTA-SZTE "Lendület" Porous Nanocomposites Research Group, Hungary*

[d] *MTA-SZTE Reaction Kinetics and Surface Chemistry Research Group, Rerrich Béla tér 1., H-6720 Szeged, Hungary*

This journal is © the Owner Societies 2013

Phys. Chem. Chem. Phys., 2013, **15**, 15917–15925 | **15917**

Gold-containing titania nanotubes were found to display higher activity in the photo-oxidation of acetaldehyde,[20] the water-gas shift reaction[22] and CO oxidation[23,24] than the Degussa P-25 catalyst. TiO$_2$ nanofibers decorated either with Pt or Pd nanoparticles show excellent photocatalytic behavior as demonstrated in decomposing organic dyes in water, degrading organic stains on the surface of a flexible freestanding cellulose–catalyst composite film and in generating hydrogen from ethanol using both suspended and immobilized catalysts.[25]

Transition metal based catalysts are widely used in the reaction of CO and H$_2$ to form linear aliphatic hydrocarbons with a broad molecular weight distribution.[26] Co and Fe are two commercially used metal catalysts for Fischer–Tropsch (FT) synthesis. Co is preferred over Fe due to its greater activity, higher chain growth probability and lower water-gas shift activity. However, Co is more expensive than Fe;[27,28] therefore, the optimal design of a Co FT catalyst is essential for practical applications. Recently, the application of various metal carbonyls to prepare catalysts for the hydrogenation of carbon monoxide has attracted great interest.[29] Extensive studies have been made on the reactivity of cobalt carbonyl compounds with the surface of SiO$_2$[30,31] and various oxide supports.[32] On the other hand, no studies have addressed the behavior of cobalt carbonyl on a titanate nanowire support until now.

In our scientific program we explore the fabrication and properties of size-controlled Co nanoparticles supported on titanate nanowires. The low-temperature decomposition of metal carbonyls is an elegant way to produce metal nanoparticles on substrates[30,33,34] (comparable similar methods are photo-induced[35] and electron-assisted[36–39] metal–CO bond cleavage in carbonyl compounds). The main advantage of low temperature carbonyl decomposition is that no high temperature calcination is necessary. Therefore, adverse effects frequently occurring during more conventional metal deposition processes (e.g. wet impregnation) like the sintering of Co nanoclusters and the destruction of the support structure can be avoided. Moreover, surface Co$_2$O$_3$ formation can also be avoided this way, which is important because this species cannot be reduced completely even at high temperatures (800–1000 K).

The goal of the present work is to provide the first comprehensive picture about the physical chemistry of cobalt deposition onto titanate nanowires by low temperature cobalt carbonyl decomposition. Moreover, we report an unexpected new finding that the stabilization pathway of cobalt on titanate nanowires is different for low and high metal loadings.

Experimental

The titanate nanowires were prepared by mixing 2 g of anatase into 140 cm^3 of 10 M aqueous NaOH solution until a white suspension was obtained, aging the suspension in a closed, cylindrical, Teflon-lined autoclave at 400 K for 1–72 h while rotating the whole autoclave intensively at 60 rpm around its short axis, and finally washing the product with deionized water and neutralizing with 0.1 M HCl acid solution to reach pH = 7; at this point, the titanate nanowire slurry was filtered and dried in air at 353 K.[13]

The impurity level of the produced nanocomposites was less than 1%. The foreign elements determined using X-ray photoelectron spectroscopy (XPS) were C, Ca, and Na that remained in the product from the preparation process.

The surface deposition of dicobalt octacarbonyl (Co$_2$(CO)$_8$) was carried out in a fluidized bed reactor designed for control experiments at low temperatures.[40] Co$_2$(CO)$_8$ was supplied by Fluka Chemie AG and used without further purification. Owing to its sensitivity to air it was stored under CO and moved into the sublimation chamber through a glovebox. Before the carbonylation process the titanate nanowires were thermally treated for 1 hour in nitrogen at 773 K. XPS and FT-IR analysis evidenced that the weakly adsorbed water and OH groups were removed during the heat treatment. The ordered TiO$_2$ anatase structure starts to develop at this temperature.[25,41,42] Energy dispersive X-ray fluorescence spectrometry (EDS) (Hitachi S4700 Scanning Electron Microscope (SEM) with an integrated R%ntec QX2 EDS Detector; 20 kV accelerating voltage) was used to determine the cobalt content of the nanowires. By increasing the carbonylation time we obtained samples with different cobalt contents: 2 and 4 wt%. For comparison, in certain cases the freshly prepared Co containing titanate nanowires were oxidized in an O$_2$ atmosphere at 600 K for 60 min and were reduced in H$_2$ at 600 K for 60 min, respectively, in the preparation chamber of the XPS.

Temperature programmed reaction spectroscopy (TPRS) and parallel thermogravimetric measurements were carried out in a Netzsch STA 409 PC microbalance connected to a Pfeiffer QMS 200 mass spectrometer system. The samples were heated with a heating rate of 10 K min^{-1} from 300 K up to 878 K in a He 4.6 stream (40 ml min^{-1}).

X-ray photoelectron spectra (XPS) were obtained using a SPECS instrument equipped with a PHOIBOS 150 MCD 9 hemispherical analyzer. The sample preparation chamber was directly connected to the measuring chamber to avoid the contamination of samples between the steps. The freshly prepared cobalt carbonyl containing titanate nanowires were placed into the preparation chamber where the in situ decomposition of carbonyl was carried out, then the sample was moved into the measuring chamber. The Al Kα radiation ($h\nu$ = 1486.6 eV) of a dual anode X-ray gun was used as the excitation source. The gun was operated at the power of 210 W (14 kV, 15 mA). The analyzer was operated in the FAT mode with a 20 eV pass energy. The energy step was 25 meV, and electrons were collected for 100 ms in one channel. Typically five scans were summed to get a single high-resolution spectrum. For binding energy reference the Ti 2p$_{3/2}$ maximum (458.9 eV) was used. The same data were obtained when C 1s (adventitious carbon at 284.9 eV) or O 1s lattice oxygen (530.1 eV) was used as the reference. For spectrum acquisition and evaluation both manufacturer's (SpecsLab2) and commercial (CasaXPS, Origin) software packages were used.

IR studies in reflection mode were performed in a high vacuum system. The samples were pressed onto a tantalum mesh.

15918 | *Phys. Chem. Chem. Phys.*, 2013, **15**, 15917–15925

This journal is © the Owner Societies 2013

The mesh was fixed to the bottom of a conventional UHV sample manipulator. It was resistively heated and the temperature of the sample was measured with a NiCr–Ni thermocouple spot welded directly to the mesh. IR spectra were recorded on a Genesis (Mattson) FTIR spectrometer. DRIFT spectra were recorded on an Agilent CARY-670 spectrometer equipped with a diffuse reflectance attachment (Thermo Electron Corporation) with BaF_2 windows. Typically 16–256 scans were registered at a spectral resolution of 1 cm^{-1}. The whole optical path was purged with CO_2- and H_2O-free air generated by a Whatman purge gas generator. The reference sample was KBr, treated in oxygen at 500 K for 20 min, then in a He atmosphere for 40 min. He 4.6 gas was used for inner purging in each experiment. The residual water contamination in He was frozen out with liquid nitrogen in a 1/8″ diameter copper tube trap.

UV-Vis diffuse reflectance spectra were obtained relative to the reflectance of a standard ($BaSO_4$) using an UV/Vis spectrophotometer (OCEAN OPTICS, Typ.USB 2000) equipped with a diffuse reflectance sampling accessory. The samples were pressed into pellets of 2 g $BaSO_4$ and 50 mg of the titanate material.

The morphology of the pristine and modified titanate nanostructures was characterized using transmission electron microscopy (FEI Tecnai G^2 20 X-Twin; 200 kV operation voltage, 180 000× magnification, 125 pm per pixel resolution). X-ray diffractometry (Rigaku MiniFlexII; Cu Kα) and the electron diffraction technique were used for crystal structure and crystallinity determinations. The Co particle size distribution was determined by image analysis of the HRTEM pictures using the ImageJ software. At least five representative images of equal magnification, taken at different spots of the TEM grid were first subjected to rolling ball background subtraction and contrast enhancement; then the diameter of the metal nanoparticles in the image was manually measured against the calibrated TEM scalebar. Each diameter distribution histogram was constructed from 200 individual nanoparticle diameters.

Results and discussion

The hydrothermal synthesis of titanate nanowires is an established method in our laboratory.[13] The properties of the product were checked by routine TEM, SEM, XRD and N_2 adsorption methods (not shown here) and found to agree with previously published data.[42] The detailed physico-chemical characterization of cobalt loaded titanate nanowires will be reported below in the following order: (i) $Co_2(CO)_8$ decomposition, (ii) titanate optical properties, (iii) detailed XPS characterization of the system and (iv) product morphology.

Cobalt carbonyl adsorbed on protonated titanate nanowires was characterized using FT-IR spectroscopy. In the solid state the structure of $Co_2(CO)_8$ is of C_{2v} point group symmetry involving a pair of bridging CO groups. The IR spectrum of adsorbed carbonyl at 323 K is displayed in Fig. 1. This spectrum is very similar to that observed in heptane solution[43] and it is close to that obtained on porous silica.[44] The observed deviations can be attributed to differences in the substrate effect and
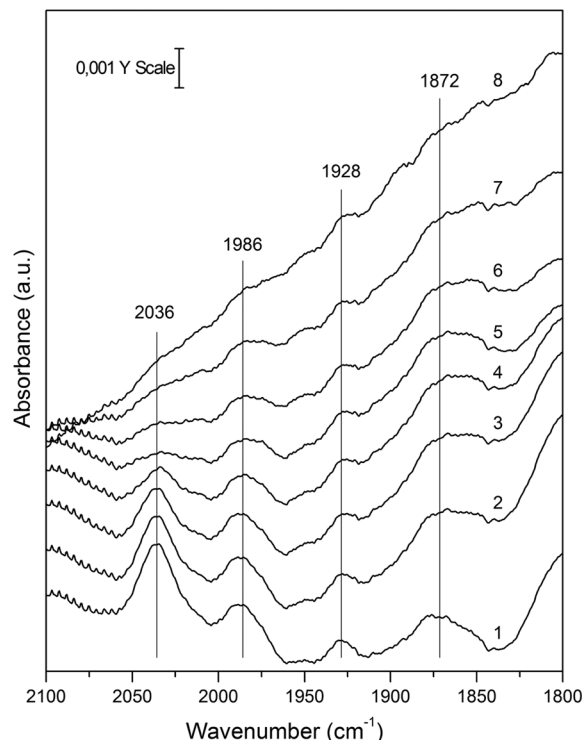

Fig. 1 FTIR spectra of adsorbed $Co_2(CO)_8$ on protonated titanate nanowire and heated with 20 K min^{-1} in He at different temperatures: 1–323 K, 2–373 K, 3–423 K, 4–473 K, 5–523 K, 6–573 K, 7–623 K, 8–673 K. Resolution: 1 cm^{-1}, number of scans: 16. Spectra were taken at given temperatures.

the different degrees of the isomerization process. Two strong bands were observed at 1986 and 2036 cm^{-1} and weak and broad bands were detected at 1928 and 1872 cm^{-1}, respectively. When the carbonyl-containing surface was heated to higher temperatures, all bands decreased in intensity. The characteristic bands disappeared at about 623 K indicating the completion of the $Co_2(CO)_8$ decomposition process.

The decarbonylation process was monitored using temperature programmed reaction spectroscopy (TPRS) as well. The sample was heated linearly (the heating rate was 10 K min^{-1}), the gas phase was monitored using mass spectrometry, and the weight loss was simultaneously measured using a microbalance. The results are shown in Fig. 2 at 4 wt% metal content. The main decomposition product in the gas phase was CO_2. Traces of CO, water and masses at 16 amu were also detected. CO_2 evolution was observed from 420 K and finished around 550 K. The weight loss measured during the heating procedure is presented as an inset in Fig. 2. A significant drop in the TG curve coincides well with the formation of CO_2 as evidenced by mass spectrometry. The fact that mainly CO_2 was formed during decarbonylation can be explained by the reaction of CO ligands with surface oxygen. This oxygen removal step contributes to the creation of oxygen vacancies in the nanowire structure significantly. Such behavior is typical for titania type catalysts where the oxide can easily be reduced and reoxidized. We note that above 650 K the remaining carbon containing species react with surface oxygen to form CO_2 and small
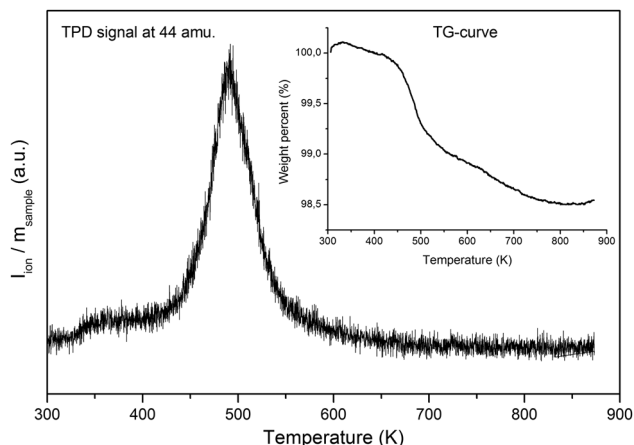
This journal is © the Owner Societies 2013

Phys. Chem. Chem. Phys., 2013, 15, 15917–15925 | 15919

Fig. 2 Ion-flow curves (TPRS) and thermal gravimetric curve (TG) of $Co_2(CO)_8$ covered titania nanowires. Mass spectrometric intensity at 44 amu was recorded during the linear heating of titanate nanowires. The insert shows the TG of $Co_2(CO)_8$ covered nanowires during linear heating. The samples were heated with a heating rate of 10 K min^{-1} from 300 K up to 878 K in He 4.6 stream (40 ml min^{-1}).
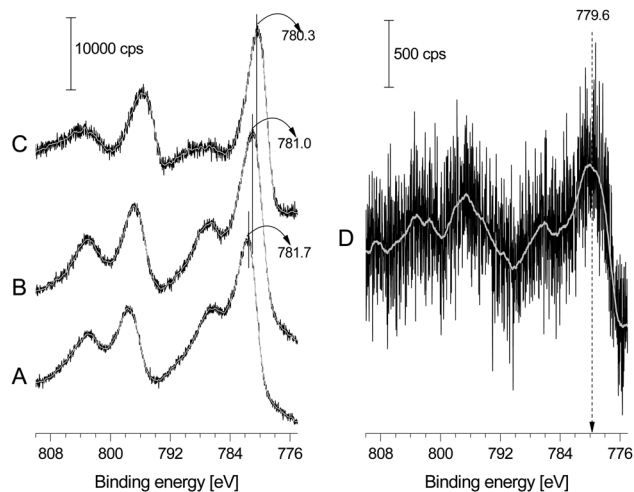

Fig. 3 Co 2p photoemission spectra: (A) as received carbonylated titanate nanowire and (B) decarbonylated sample at 4% metal content (decomposed sample at 600 K in N_2 atmosphere for 10 min). (C) Decarbonylated sample after oxidation at 600 K for 60 min, and (D) after reduction at 600 K for 60 min.

hydrocarbons in the gas phase. This agrees with the high temperature weight loss of the sample. Co-containing components were not detected in the gas phase during decomposition. Qualitatively the same FT-IR and TPRS features were observed in the case of 2 wt% metal content. However, at this small metal loading there were no Co clusters visible in the HRTEM images.

Let us focus now on the optical properties of cobalt-decorated titanate nanowires. We measured the diffuse reflectance UV-Vis spectra to determine the changes in the band gap of titanate nanowires after the decomposition of cobalt carbonyl. The color of the samples changed from yellowish to intense yellow with increasing carbonylation time. Correspondingly, the absorption edge shifted into the visible range. The band gap energy (E_g) was calculated according to Beranek and Kisch[45] who used the equation $\alpha = A(h\nu - E_g)^n/h\nu$, where α is the absorption coefficient, A is a constant, $h\nu$ is the energy of light and n is a constant depending on the nature of electron transition. Assuming an indirect band gap ($n = 2$) for TiO_2,[46] with α proportional to $F(R_\infty)$ the band gap energy can be obtained from the Kubelka–Munk plots (not shown) of $[F(R_\infty)/h\nu]^{1/2}$ vs. $h\nu$ as the interception at $[F(R_\infty)/h\nu]^{1/2} = 0$ of the extrapolated linear part of the plot. The band gap for pure titanate nanowires was 3.14 eV, while that for Co-doped titanates was significantly less, 2.48 for 2 wt% and 2.41 eV for 4 wt% Co content. No significant changes were observed above 2 wt% metal loading.

The band gap of nanosize anatase TiO_2 is 3.20 eV.[47–49] In our reference experiment the band gap of high surface area commercial TiO_2 (Degussa P25) decreased to 3.03 eV upon depositing 2 wt% cobalt onto it by low temperature $Co_2(CO)_8$ decomposition. The more pronounced decrease of the band gap of titanate nanowires upon loading with 2 wt% Co suggests a very strong electronic interaction between the titanate nanowire framework and cobalt, which may eventually result in an ion exchange process similar to that occurring in silver loaded titanate nanotubes.[16] On silver exchanged titanates, the formation of the $Ag^+(CO)_n$ ($n = 1, 2$) species has been revealed.

Positively charged cobalt in the ion exchange position could also be formed during ion exchange which is demonstrated in our XPS as well. After decomposition of carbonyl the Co $2p_{3/2}$ can be detected at 781.5 eV and the $2p_{1/2}$ orbital located at 797.3 eV, which with satellites (at 787.8 and 804.0 eV) are characteristic for the Co^{2+} ion.[50,51]

Detailed XPS measurements were performed on the 4 wt% cobalt containing sample (Fig. 3). In the "as received sample" the $2p_{3/2}$ photoemission appeared at 781.7 eV, the $2p_{1/2}$ emission was located at 797.5 eV and strong satellite structures were also present for $2p_{3/2}$ and $2p_{1/2}$, respectively (Fig. 3A). The spin orbit coupling (15.8 eV) is almost the same as for Co^{2+} and a little bit higher than for metallic Co.[33,52,53] New O 1s XPS peaks appeared in addition to the bulk O^{2-} signal after carbonylation at 531.7 and 532.6 eV, respectively (Fig. 4A). The dominant emission besides titanate lattice oxygen (530.1 eV) is at 531.7 eV, while the peak at 532.6 eV has much less intensity. An intense C 1s signal appeared due to the carbonyl fragment at 289.6 eV and a smaller one at 288.6 eV (Fig. 5A). These two emissions can be assigned to adsorbed carbonyl fragments in two orientations. When the carbonylated sample was heated to 600 K at which CO_2 is already formed (Fig. 2), the intensity of Co 2p did not decrease but the peak shifted significantly to lower binding energies by 0.7 eV (Fig. 3B). Interestingly, the binding energy positions of satellites remained. At this temperature the intensities of the O 1s peaks representing different orientations and/or different carbonyls ($Co_2(CO)_8$, $Co_4(CO)_{12}$) at 531.7 and 532.6 eV for O 1s diminished or decreased significantly (Fig. 4B). The remaining small intensity emissions could be assigned to some undecomposed carbonyls or "bridging O" and "top O" groups on the titanate surface besides bulk O^{2-} at 530.1 eV.[54] The O 1s feature did not change after oxidation (Fig. 4C) nor after further reduction (Fig. 4D) of the sample at 600 K for 60 min. Similarly to the O 1s photoemissions, the intensity of C 1s signals for carbonyl species also diminished
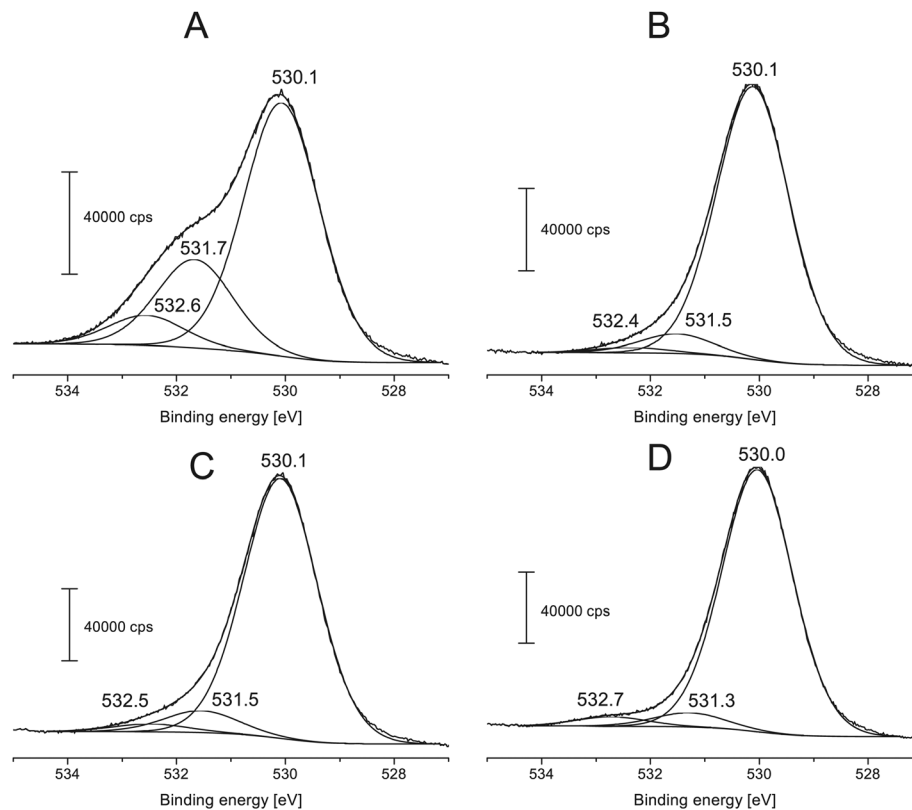
Fig. 4 O 1s photoemission spectra: (A) obtained after carbonylation (as received) and (B) after decarbonylation (600 K in N_2 atmosphere for 60 min), (C) oxidation at 600 K for 60 min, and (D) reduction at 600 K for 60 min.

after decarbonylation (Fig. 5B). The observed small intensity C 1s peaks could be attributed to the still intact carbonyls and/or different carbon species remaining from the decomposition of carbonyl. The peak at 285.0 eV is due to residual carbon contamination of titanate nanowires.

The findings discussed above suggest that decarbonylation occurs between 300 and 600 K. The observed Co 2p photoemission peaks are higher than those of pure metallic Co and in addition the "oxide-like" satellite structure remained, although the intensities of the O 1s peaks at 531.7 eV and 532.6 eV decreased drastically. When the decarbonylated surface was kept in O_2 atmosphere at 600 K for 60 min, the Co $2p_{3/2}$ peak position moved to lower binding energies to 780.3 eV and its intensity decreased (Fig. 3C). These two changes can be attributed to the formation of oxides[52,55] and the agglomeration/encapsulation of clusters.[29,56–58] When the sample was treated further in a H_2 atmosphere at 600 K for 60 min a low intensity Co $2p_{3/2}$ peak appeared at 779.6 eV indicating the tendency for the reduction of the Co species[29,33,52,53] (Fig. 3D). The intensity changes also correlate with the coalescence and diffusion into the bulk.

Very recently we observed the similar, unexpectedly high binding energy photoemission of gold stabilized in titanate nanowires and nanotubes in atomically dispersed states complexed with oxygen vacancies.[17–19] An atomically dispersed state was observed for Au atoms on TiO_2(110) at low temperature.[59] In this case, Au deposited as Au^+ at 1 eV impact energy on rutile

TiO_2 samples was studied over the temperature range between 115 K and 800 K, and both near-stoichiometric UHV-annealed TiO_2 and TiO_2 with high density of oxygen vacancies were created by He^+ bombardment. At low temperatures, Au was atomically dispersed (Au $4f_{7/2}$ at 85.8 eV), shifting into complexes with oxygen vacancies for T_{anneal} around room temperature (85.4 eV) and finally agglomerating into small clusters above 450 K (84.5 eV). The main message of these experiments is that small cobalt clusters could be stabilized in a similar manner in the structure of titanate nanowires.

Due to the preparation method of titanate nanowires (structural water release during heat treatment) and CO_2 formation upon carbonyl decomposition the nanowires may contain more defects than reduced commercial titania. The presence of defects was indirectly evidenced by the TPRS measurements discussed above. Therefore, we may suppose that after carbonyl decomposition cobalt is found in a strongly oxygen vacant environment with high dispersion and small cluster size (2–5 nm) (see Fig. 8A). Core level shifts due to the nanoparticle size must be considered in the interpretation of such XPS.[60] Initial effects like the intrinsic size effect caused by the reduced average coordination number of surface atoms in small particles lead to decreasing binding energy for core level electrons. Furthermore, electron exchange with the support can change the binding energy of electrons emitted from the nanoparticle. The binding energy is also influenced by relaxation energy. This "final-state" effect depends on the particle size, too.[60]
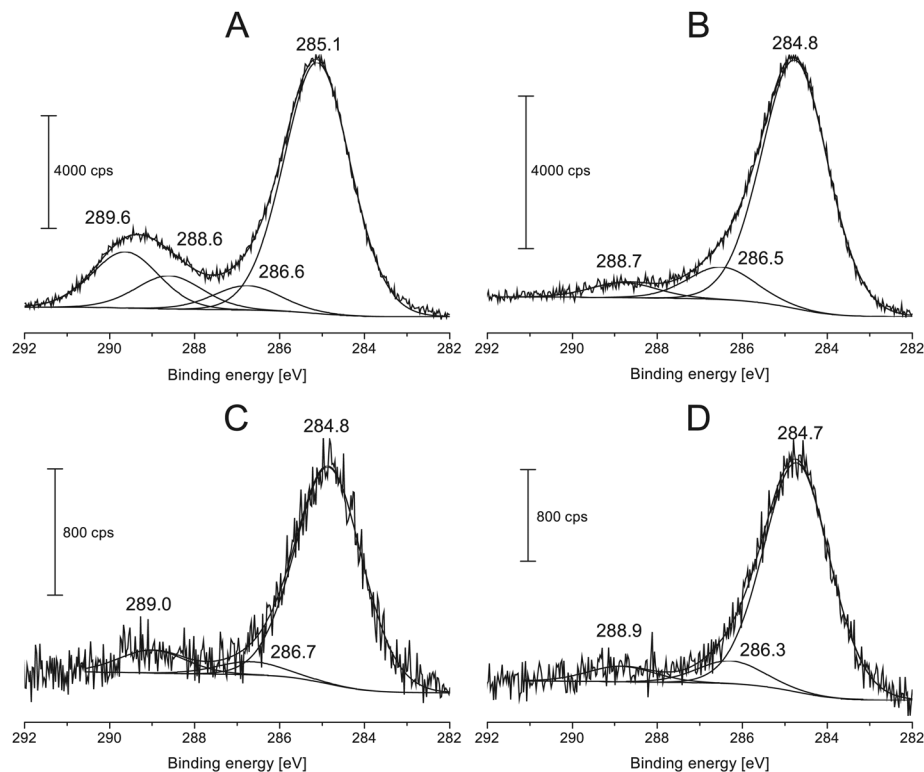
Fig. 5 C 1s photoemission spectra: (A) obtained after carbonylation (as received) and (B) after decarbonylation (600 K in N$_2$ atmosphere for 60 min), (C) oxidation at 600 K for 60 min, and (D) reduction at 600 K for 60 min.

The stabilization process of small clusters may also involve an electron transfer step from the cobalt to the titanate nanostructure, which is manifested in a higher binding energy position of Co. This hypothesis is also supported by previous results achieved on similar systems. Recently, titanium dioxide TiO$_2$(110) surfaces with Pt adatoms were examined using a noncontact atomic force microscope (NC-AFM) and Kelvin probe force microscope (KPFM). Platinum clusters with diameters of 2–3 nm were obtained. The work function decrease was interpreted using an electric dipole moment directed toward the vacuum, as a result of electron transfer from the adatom to the TiO$_2$ substrate.[61,62] Moreover, similar phenomena may occur in the Rh–titanate nanosystem as well. Rh adatoms on Ti atoms and O atoms are mobile while the adatoms in the O atom vacancies are not. A rhodium adatom in an O atom vacancy is in contact with two Ti atoms and therefore, the electron transfer can be enhanced.[21]

We conclude the characterization of cobalt loaded titanate nanowires by reporting on their morphology. XRD and ED measurements in Fig. 6 confirm that the nanowire structure is stable up to 573 K. The protonated titanate phase was identified on the basis of its reflections with Miller indices of (001), (011), (300), (203) and (401) found at 10.5°, 25.7°, 29.9°, 34.2° and 43.9°, respectively. When the protonated titanate was heated to 773 K to remove all hydroxyl species some TiO$_2$ in the anatase phase developed as indicated by the appearance of the characteristic anatase reflections (101), (004), (200), (105), (211) and (204) at 25.3°, 37.8°, 48.1°, 53.9°, 55.1° and 62.4°, respectively.

Transmission electron microscopy (Fig. 7A) revealed that the nanowires preserve their curled-up shape during heat treatment up to 873 K. However, more and more textural discontinuities can be observed at higher temperatures. The holey structure can be attributed to the local density changes accompanying the continuous transformation of the protonated titanate nanowires into the more compact TiO$_2$ (anatase) phase.

The carbonylated surface was heated *in situ* to 600 K to decompose Co$_2$(CO)$_8$ on the titanate support and the samples were scrutinized to search for Co clusters. For up to 2 wt% metal content Co nanoparticles could not be located by HRTEM. This is in agreement with diffuse reflectance UV-Vis spectrometric data which also suggested that the system is characterized by ion exchange between cobalt and protonated titanate nanowires instead of Co nanoparticle formation at this metal content.

At 4 wt% Co loading the formation of cobalt nanoparticles is evident; the clusters are clearly identified in HRTEM Fig. 7B and C corresponding to as-synthesized and 873 K flashed Co-containing titanate nanowires, respectively. The corresponding cobalt nanoparticle diameter distributions are depicted in Fig. 8A and B, respectively. The high temperature treatment shifted the diameter distribution upwards and broadened it, indicating that a cobalt agglomeration process was initiated thermally.

The driving force of the shift from the ion exchange to the cluster formation cobalt stabilization mechanism is probably the saturation of the surface ion exchange positions at the early stages of the carbonyl decomposition process
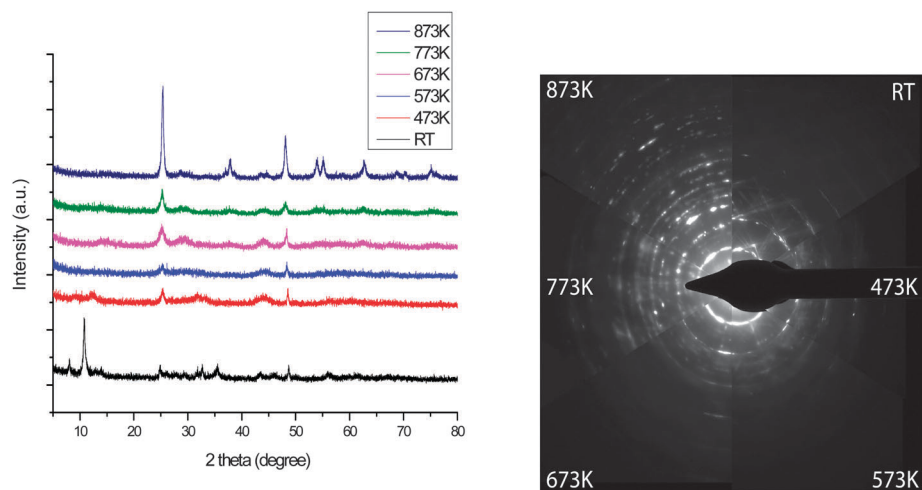
15922 | *Phys. Chem. Chem. Phys.*, 2013, **15**, 15917–15925

This journal is © the Owner Societies 2013

Fig. 6 XRD and ED of protonated nanowires at different temperatures.

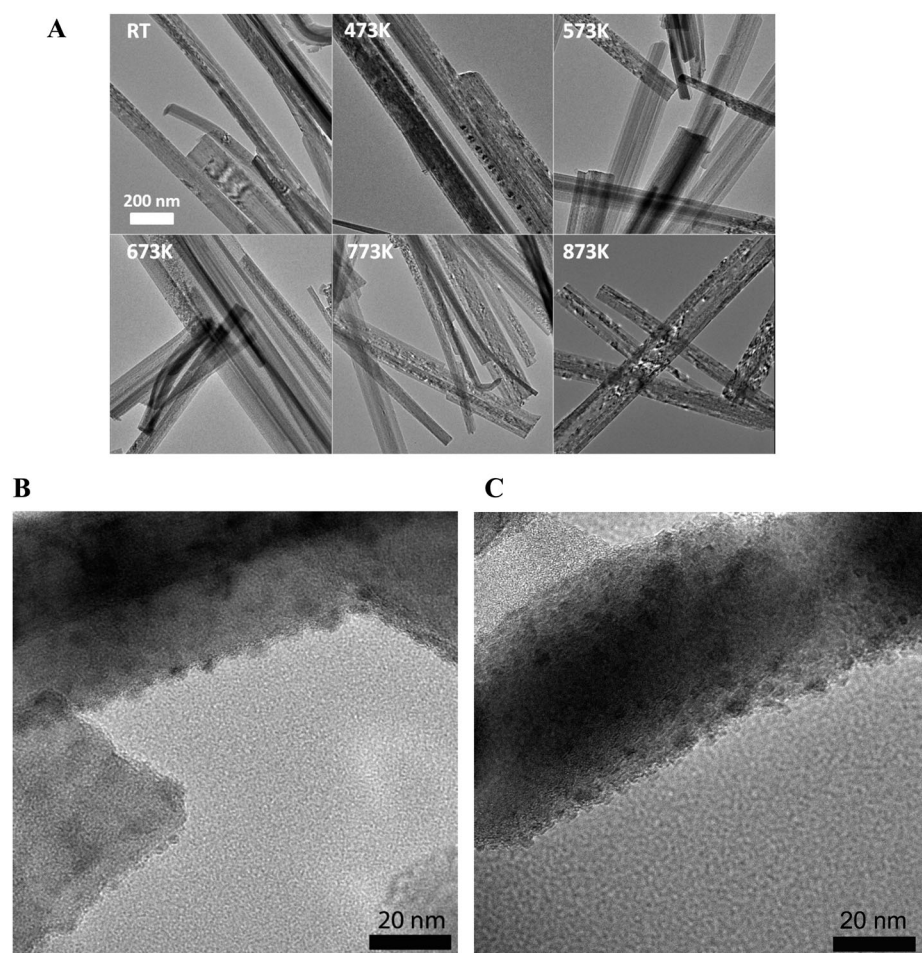**Fig. 7** TEM images of protonated titanate nanowire treated at different temperatures for 60 min in air (A), after decomposition of $Co_2(CO)_8$ on protonated titanate nanowire (B) and after flashing the $Co_2(CO)_8$ covered sample up to 873 K. The metal content in parts (B) and (C) was 4 wt%.

(up to approx. 2 wt% Co loading). Once the available positions are filled up, subsequently deposited cobalt is stabilized in the cluster form at oxygen vacancies formed during the $Co_2(CO)_8$ decomposition step in the titania structure.

The as-synthesized 4 wt% Co loaded sample contains mostly cobalt clusters in the 2–6 nm range which could be a favorable size regime for some important catalytic reactions. Therefore, we performed a simple proof-of-concept type ethanol decomposition
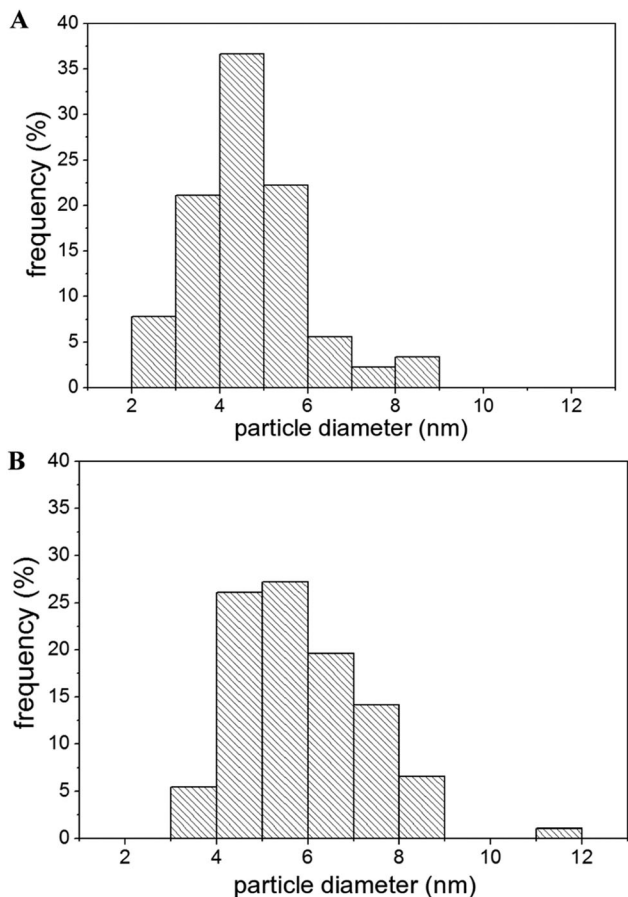
This journal is © the Owner Societies 2013

Phys. Chem. Chem. Phys., 2013, **15**, 15917–15925 | **15923**

Fig. 8 Diameter distribution of Co nanoparticles (A) obtained after decomposition of $Co_2(CO)_8$ on protonated titanate nanowire (600 K in N_2 atmosphere for 60 min), and (B) after flashing the $Co_2(CO)_8$ covered sample up to 873 K. The samples were heated with a heating rate of 10 K min^{-1} in He 4.6 stream (40 ml min^{-1}).

test reaction on the 4 wt% Co loaded titanate nanowire samples to test their future applicability as heterogeneous catalysts. The ethanol conversion was 35–40% with 40% hydrogen selectivity at 605 K on the as-synthesized sample (Fig. 8A). The catalytic activity decreased in the heat-treated sample (Fig. 8B). A detailed study of the catalytic performance of Co nanocluster loaded titanate nanowires is currently underway on the basis of these first results and will be reported in a future communication.

Conclusions

We presented the first comprehensive study on the structure of cobalt-loaded titanate nanowires obtained by the low-temperature thermal decomposition of $Co_2(CO)_8$. Co nanoparticles were prepared and characterized on protonated titanate nanowires. The carbonylation was carried out under inert atmosphere in a fluidized bed reactor. The decarbonylation processes were monitored by FT-IR spectroscopy and microbalance combined with temperature programmed reaction mass spectrometry. CO_2 was the main decomposition product in the gas phase which was interpreted as a sign of oxygen vacancy formation in

the titania support. The decomposition of $Co_2(CO)_8$ was almost complete at 550–600 K. Depending on metal loading, Co was stabilized on titanate nanowires either in the Co^{2+} form by ion exchange or by cluster formation. The chemical nature and morphology of cobalt particles were characterized using X-ray photoelectron spectroscopy and HRTEM.

The optical properties of Co containing titanate nanowires were explored by means of ultraviolet-visible diffuse reflectance spectroscopy. The band gap decreased from 3.14 eV to 2.41 eV with increasing Co content for up to 2 wt% cobalt content. This drastic reduction was not observed when Co was deposited in a similar way on commercial TiO_2. The significant change in the band gap due to Co loading suggests that cobalt is stabilized in the structure by ion exchange up to 2 wt% loading. The reduced band gap may be exploited by future photocatalytic applications of Co-decorated titanate nanowires.

Higher cobalt loadings (4 wt%) lead to the formation of dispersed Co nanoparticles complexed with oxygen vacancies. The shift from ion-exchange to cluster formation stabilization pathway is suggested to be due to the saturation of available surface ion exchange positions in the titanate nanowires. The average Co particle sizes were between 2 and 6 nm, which could be a favorable regime for some important low-temperature catalytic reactions, $e.g.$ ethanol transformation.

References

1 M. Hodos, E. Horváth, H. Haspel, Á. Kukovecz, Z. Kónya and I. Kiricsi, *Chem. Phys. Lett.*, 2004, **399**, 512–515.
2 G. K. Mor, K. Shankar, M. Aulose, O. K. Varghese and C. A. Grimes, *Nano Lett.*, 2005, **5**, 191–193.
3 S. Kubota, K. Johkura, K. Asanuma, Y. Okouchi, N. Ogiwara, K. Sasaki and T. Kasuga, *J. Mater. Sci.: Mater. Med.*, 2004, **15**, 1031–1035.
4 L. Kavan, M. Kalbac, M. Zukalova, I. Exnar, V. Lorenzen, R. Nesper and M. Graetzel, *Chem. Mater.*, 2004, **16**, 477–485.
5 D. Bavykin, A. A. Lapkin, P. K. Plucinski, J. M. Friderich and F. C. Walsh, *J. Phys. Chem. B*, 2005, **109**, 19422–19427.
6 R. Huang, F. Chung and E. M. Kelder, *J. Electrochem. Soc.*, 2006, **153**, A1459–A1465.
7 P. Yang, D. K. Zhong, M. Yuan, A. H. Rice, D. R. Gamelin and C. K. Luscombe, *Phys. Chem. Chem. Phys.*, 2013, **15**, 4566–4572.

15924 | *Phys. Chem. Chem. Phys.*, 2013, **15**, 15917–15925

This journal is © the Owner Societies 2013

8 M. T. Byrne, J. M. McCarty, M. Bent, R. Blake, Y. K. Gun'ko, E. Horváth, Z. Kónya, Á. Kukovecz, I. Kiricsi and J. N. Coleman, *J. Mater. Chem.*, 2007, **17**, 2351–2358.

9 H.-H. Ou and S.-L. Lo, *Sep. Purif. Technol.*, 2007, **58**, 179–191.

10 L. Torrente-Murciano, A. A. Lapkin and D. Chadwick, *J. Mater. Chem.*, 2010, **20**, 6484–6489.

11 T. Kasuga, M. Hiramatsu, A. Hoson, T. Sekino and K. Niihara, *Langmuir*, 1998, **14**, 3160–3164.

12 S. Zhang, T. Y. Peng, Q. Chen, G. H. Du, G. Dawson and W. Zhou, *Phys. Rev. Lett.*, 2003, **91**, 256103–256105.

13 E. Horváth, Á. Kukovecz, Z. Kónya and I. Kiricsi, *Chem. Mater.*, 2007, **19**, 927–931.

14 T. Ohsaka, F. Izumi and Y. Fujiki, *J. Raman Spectrosc.*, 1978, **7**, 321–325.

15 X. Sun and Y. Li, *Chem.–Eur. J.*, 2003, **9**, 2229–2238.

16 F. Cesano, S. Bertarione, M. J. Uddin, G. Agostini, D. Scarano and A. Zeccina, *J. Phys. Chem. C*, 2010, **114**, 169–178.

17 Á. Kukovecz, G. Pótári, A. Oszkó, Z. Kónya, A. Erdőhelyi and J. Kiss, *Surf. Sci.*, 2011, **605**, 1048–1055.

18 A. Oszkó, G. Pótári, A. Erdőhelyi, Á. Kukovecz, Z. Kónya, I. Kiricsi and J. Kiss, *Vacuum*, 2011, **85**, 1114–1116.

19 J. Kiss, L. Óvári, A. Oszkó, G. Pótári, M. Tóth, K. Baán and A. Erdőhelyi, *Catal. Today*, 2012, **181**, 163–170.

20 S. S. Malwadkar, R. S. Gholap, S. V. Awante, P. Korake, M. G. Chaskar and N. M. Gupta, *J. Photochem. Photobiol., A*, 2009, **203**, 24–31.

21 G. Pótári, D. Madarász, L. Nagy, B. László, A. Sápi, A. Oszkó, A. Kukovecz, A. Erdőhelyi, Z. Kónya and J. Kiss, *Langmuir*, 2013, **29**, 3061–3072.

22 V. Idakiev, Z. Yuan, T. Tabakova and B.-L. Su, *Appl. Catal., A*, 2005, **281**, 149–155.

23 T. Akita, M. Okumura, K. Tanaka, K. Ohkuma, M. Kohyama, T. Koyanagi, M. Date, S. Tsubota S and M. Haruta, *SIA Surf. Interface Anal.*, 2005, **37**, 265–269.

24 M. Mendez-Cruz, J. Ramirez-Solis and R. Zanella, *Catal. Today*, 2011, **166**, 172–179.

25 M.-C. Wu, A. Sápi, A. Avila, M. Szabó, J. Hiltunen, G. Tóth, Á. Kukovecz, Z. Kónya, R. Keiski, W.-F. Su, H. Jantunen and K. Kordás, *Nano Res.*, 2011, **4**, 360–369.

26 V. Ponec, *Stud. Surf. Sci. Catal.*, 1991, **64**, 117–157.

27 M. E. Dry, *Stud. Surf. Sci. Catal.*, 2004, **152**, 196–199.

28 N. S. Gluck, Z. Ying, C. E. Bartosch and W. Ho, *J. Chem. Phys.*, 1987, **86**, 4957–4978.

29 L. Guczi, G. Boskovic and E. Kiss, *Catal. Rev.*, 2010, **52**, 133–203, and references therein.

30 S. Suvanto, T. A. Tapani, A. Pakkanen and L. Backman, *Appl. Catal., A*, 1999, **177**, 25–36.

31 Z.-j. Wang, S. Skiles, F. Yang and D. W. Goodman, *Catal. Today*, 2012, **181**, 75–81.

32 A. S. Lisitsyn, V. L. Kuznetsov and Yu. I. Yermakov, *React. Kinet. Catal. Lett.*, 1980, **14**, 445–450.

33 A. Beck, A. Horváth, A. Sárkány and L. Guczi, *Curr. Appl. Phys.*, 2006, **6**, 200–204.

34 H. Khosravian, Z. Liang, A. Uhl, M. Trenary and R. Meyer, *J. Phys. Chem. C*, 2012, **116**, 11987–11993.

35 R. C. Reul and C. H. Bartholomew, *J. Catal.*, 1984, **85**, 78–88.

36 M.-M. Walz, M. Schirmer, F. Vollnhals, T. Lukasczyk, H.-P. Steinrück and H. Marbach, *Angew. Chem., Int. Ed.*, 2010, **49**, 4669–4673.

37 K. Muthukumar, H. O. Jeschke, R. Valenti, E. Begun, J. Schwenk, F. Porrati and M. Huth, *Beilstein J. Nanotechnol.*, 2012, **3**, 546–555.

38 Z. Majzik, N. Balázs, L. Robin, M. Petukhov, B. Domenichini, S. Bourgeois and A. Berkó, *Vacuum*, 2012, **86**, 623–625.

39 P. Krüger, M. Petukhov, B. Domenichini, A. Berkó and S. Bourgeois, *J. Phys. Chem. C*, 2012, **116**, 10617–10622.

40 J. Kiviaho, M. K. Niemelä, M. Reinikainen, T. Vaara and T. A. Pakkanen, *J. Mol. Catal. A: Chem.*, 1997, **121**, 1–8.

41 M.-C. Wu, G. Tóth, A. Sápi, Z. Kónya, Á. Kukovecz, W.-F. Su and K. Kordás, *J. Nanosci. Nanotechnol.*, 2012, **12**, 1421–1426.

42 H. Haspel, N. Laufer, V. Bugris, R. Ambrus, P. Szabó-Révész and Á. Kukovecz, *J. Phys. Chem. C*, 2012, **116**, 18999–19009.

43 W. Rupilius, J. J. McCoy and M. Orchin, *Ind. Eng. Chem. Prod. Res. Dev.*, 1971, **10**, 142–145.

44 M. van Boven, N. Alemdaroglu and J. M. L. Penninger, *J. Organomet. Chem.*, 1975, **84**, 65–74.

45 R. Beranek and H. Kisch, *Photochem. Photobiol. Sci.*, 2008, **7**, 40–48.

46 H. Tang, K. Prasad, R. Sanilines, P. E. Schmid and F. Lewy, *J. Appl. Phys.*, 1994, **75**, 2042–2047.

47 S. G. Kumar and L. G. Devis, *J. Phys. Chem. A*, 2011, **115**, 13211–13241.

48 K. M. Reddy, I. V. Manorama and A. R. Reddy, *Mater. Chem. Phys.*, 2003, **78**, 239–245.

49 A. Henderson, *Surf. Sci. Rep.*, 2011, **66**, 185–297.

50 S. W. Ho, M. Horilla and D. M. Hercules, *J. Phys. Chem.*, 1999, **94**, 6396.

51 T. J. Chuang, C. R. Brundle and D. W. Rice, *Surf. Sci.*, 1976, **59**, 413.

52 S. C. Petitto, E. M. Marsh, G. A. Carson and M. A. Langell, *J. Mol. Catal. A: Chem.*, 2008, **281**, 49–58.

53 Z. Zsoldos and L. Guczi, *J. Phys. Chem.*, 1992, **96**, 9393–9400.

54 H. Perron, J. Vandenborre, C. Domain, R. Drot, J. Roques, E. Simoni, J. J. Ehrhardt and H. Catalette, *Surf. Sci.*, 2007, **601**, 518–527.

55 M. C. Biesinger, B. P. Pague, A. P. Grosvenor, L. W. M. Lau, A. R. Gerson and R. St. C. Smart, *Appl. Surf. Sci.*, 2011, **257**, 2717–2730.

56 Y. Shao, W. Chen, E. Wold and J. Paul, *Langmuir*, 1994, **10**, 178–187.

57 V. A. D. O'Shea, M. C. A. Galvan, A. E. P. Parts, J. M. Campos-Martin and J. L. G. Fierro, *Chem. Commun.*, 2011, **47**, 7131–7133.

58 R. P. Galhenage, H. Yan, S. A. Tenny, N. Park, G. Henkelman, P. Albrecht, D. R. Mullins and D. A. Chen, *J. Phys. Chem. C*, 2013, **117**, 7191–7201.

59 C. Fan, T. Wu and S. L. Anderson, *Surf. Sci.*, 2005, **578**, 5–19.

60 C. R. Henry, *Surf. Sci. Rep.*, 1998, **31**, 231–325.

61 A. Sasahara, C. L. Pang and H. Onishi, *J. Phys. Chem. B*, 2006, **110**, 13453–13457.

62 A. Sasahara, C. L. Pang and H. Onishi, *J. Phys. Chem. B*, 2006, **110**, 17584–17588.